

# SUPPORTING INFORMATION

## Radially grown graphene nanoflakes on carbon fibres as reinforcing interface for polymer composites

Anastasios Karakassides <sup>a</sup>, Abhijit Ganguly <sup>a</sup>, Kyriaki Tsirka <sup>b</sup>, Alkiviadis S. Paipetis <sup>b</sup>, Pagona  
Papakonstantinou <sup>a,\*</sup>.

<sup>a</sup> School of Engineering, Engineering Research Institute, Ulster University, Newtownabbey  
BT37 0QB, United Kingdom

<sup>b</sup> Composite and Smart Materials Laboratory, Department of Materials Science and Engineering,  
University of Ioannina, Ioannina, Greece

---

\* Corresponding author: School of Engineering, Engineering Research Institute, Ulster University, Newtownabbey BT37 0QB, United Kingdom.

E-mail address: [p.papakonstantinou@ulster.ac.uk](mailto:p.papakonstantinou@ulster.ac.uk)

## **S1. Materials**

Polyacrylonitrile based sized (PAN) carbon fibre (Torayca T700SC) tows consisting of 12,000 fibres were supplied from Toray (JP). These purchased fibres had a 1.2 wt% sizing (Bisphenol A epoxy + Unsaturated polyester) designed for epoxy and polyester matrices. Each fibre had a circular cross-section with a diameter about 7  $\mu\text{m}$ . All gases used in this study ( $\text{N}_2$ , Ar,  $\text{CH}_4$ ) were purchased by BOC UK. The conductive silver paint (PELCO Conductive Silver Paint) used for the electrical conductivity measurements was supplied by Agar Scientific Ltd.

## **S2. Direct growth of GNFs on carbon fibres**

The mw-PECVD system is a low-pressure deposition system. For that reason, the samples were placed inside a sealed vacuum chamber. After the desired pressure achieved the heating process started. One of the advantages of this system is that the heater can operate extremely fast with a heating rate of about 55-60  $^{\circ}\text{C}/\text{min}$ . So, after max. 10 min the desired temperature of 600  $^{\circ}\text{C}$  was achieved. Then, the striking process of the plasma started. The total procedure of GNFs growth was 5 minutes. 2 minutes of  $\text{N}_2/\text{Ar}$  etching and 3 mins of  $\text{CH}_4$  deposition. The microwave system is a very delicate system. In order to strike the plasma, it was necessary to have Ar flow inside the chamber. We have tried many times to strike to plasma in an  $\text{N}_2$  environment but it was not possible. For that reason, we were striking the plasma at Ar environment and gradually replaced the Ar with  $\text{N}_2$  as fast we could ( $\sim 1$  min) from the time the plasma appeared.

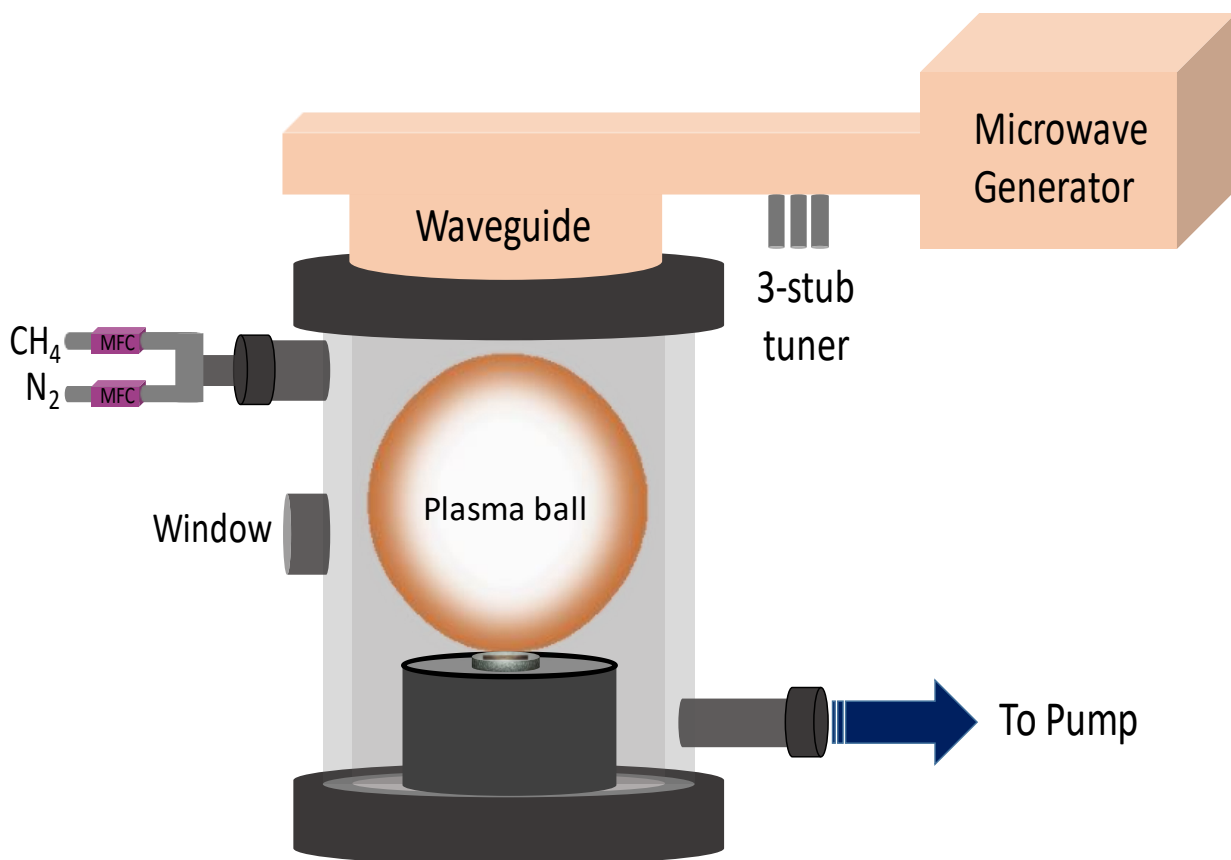


**Figure S1.** Schematic diagram of the preparation process

### S3. Raman analysis of the GNFs/CF hybrids

Raman characterisation was used to assess the quality and uniformity of GNFs on CF using an excitation wavelength of 532 nm (RL532C laser source) at a Renishaw Invia Qontor system.

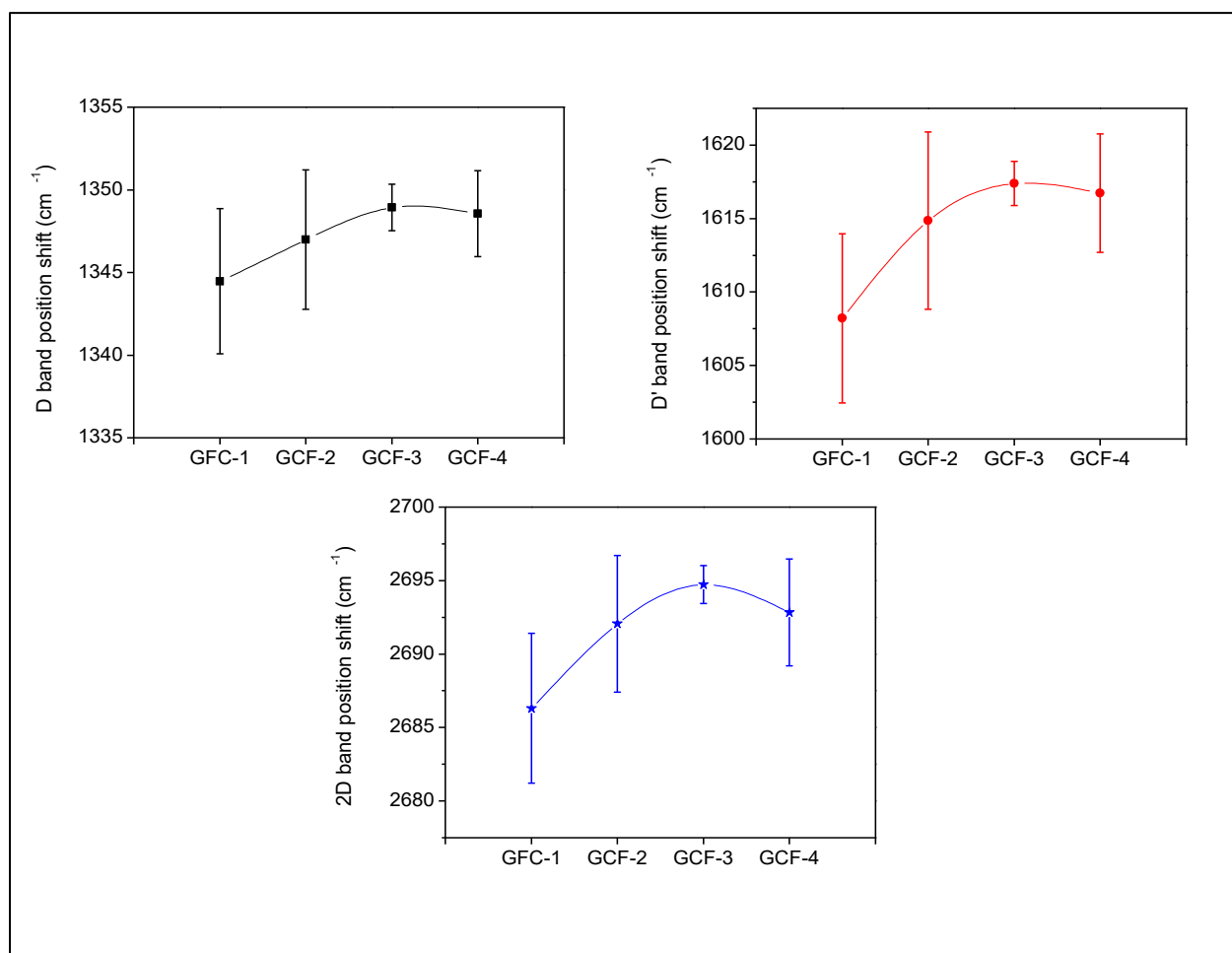


**Figure S2.** Raman characterization of single carbon fibres. Position shift of characteristic bands (D, D' and 2D). Error bars represent standard deviation from at least 20 independent measurements.

**Table S1.** Position shift of characteristic bands

GNFs/CF	D shift	D' shift	2D shift
GCF-1	$1344 \pm 4$	$1608 \pm 6$	$2686 \pm 5$
GCF-2	$1347 \pm 4$	$1615 \pm 6$	$2692 \pm 5$
GCF-3	$1349 \pm 1$	$1617 \pm 1$	$2695 \pm 1$
GCF-4	$1349 \pm 3$	$1617 \pm 4$	$2693 \pm 4$

### S3.1 Raman spectra along the GNFs/CF hybrid fibre length

Raman spectra along the fibre length were acquired as a means for check uniformity of the GNF coating. Representative graphs of one individual fibre (GCF-3 ) are presented below.

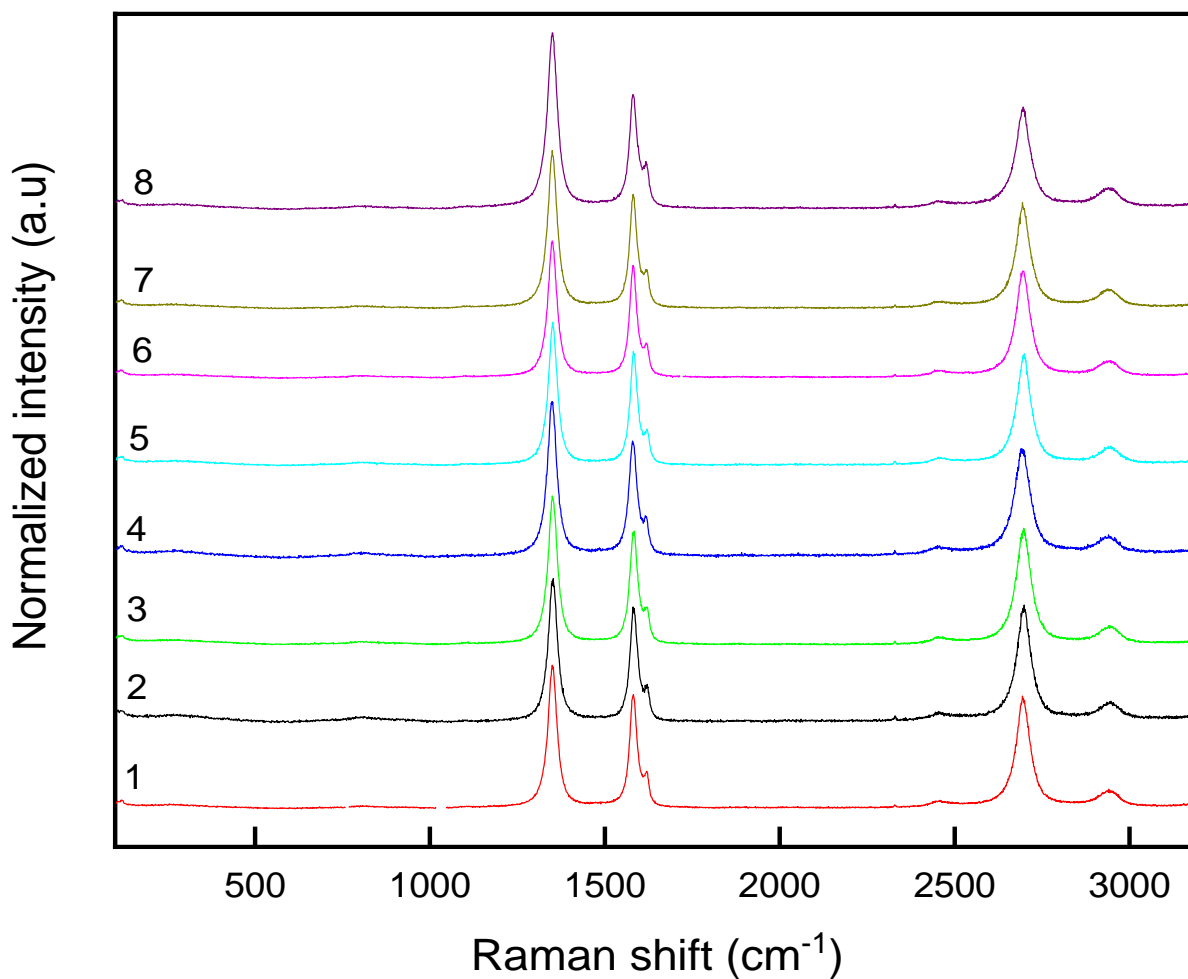


**Figure S3.** Representative Raman spectra acquired along the GCF3 hybrid fibre length to access its uniformity.

#### S4. Estimation of fibre diameters using Renishaw Invia Qontor system

Also, the diameters of single carbon fibres separated from carbon fibre yarn, were determined by optical analysis with the help of an external image processing software (ImageJ). Firstly, an image of each fibre was acquired from the microscope of the Raman system and then, with the help of an external image processing software (ImageJ) 20 different diameter measurements along each fibre's centre were acquired (**Figure S3**). Even though the scatter in the diameter of the fibres seemed not to be significant ( $<9\%$ ) (**Table S2**), the effect of this scatter was important in the calculation of tensile strength. This is because the tensile strength is inversely proportional to the square of the diameter (Equations 1, 2).

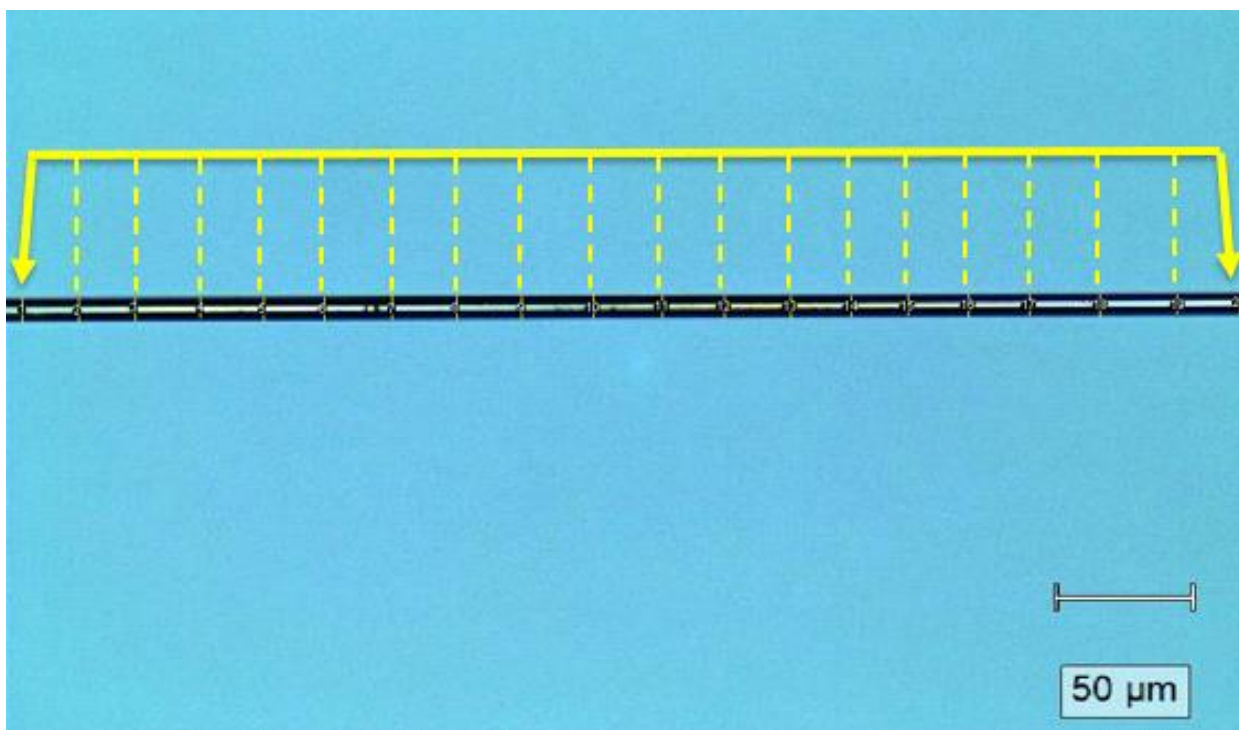


**Figure S4.** Representative optical image for determination of the single carbon fibre diameter.

**Table S2.** Percentage of difference in diameter of the fibres along their length

GNFs/CF	Percentage of difference in diameter (%)
GCF-1	4.2
GCF-2	3.3
GCF-3	4.6
GCF-4	4.2

## **S5. SEM observations of GNFs/CF hybrids**

The as-grown samples were observed with a field emission scanning electron microscope FESEM, (HITACHI SU5000) operated at an accelerating voltage of 15kV and 20kV. Photos were acquired along the yarn in order to determine possible changes at the grown morphology. The samples were extremely conductive and for that reason no additional metal coating was needed.

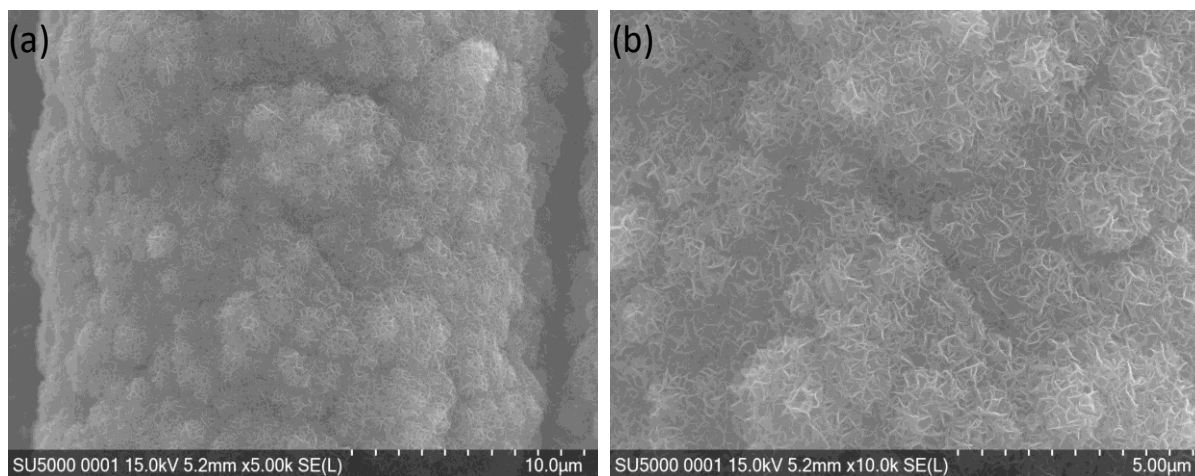


**Figure S5.** SEM micrographs of unsized CF coated with GNFs possessing a spherule-like morphology grown at 800 W @ 600 °C.

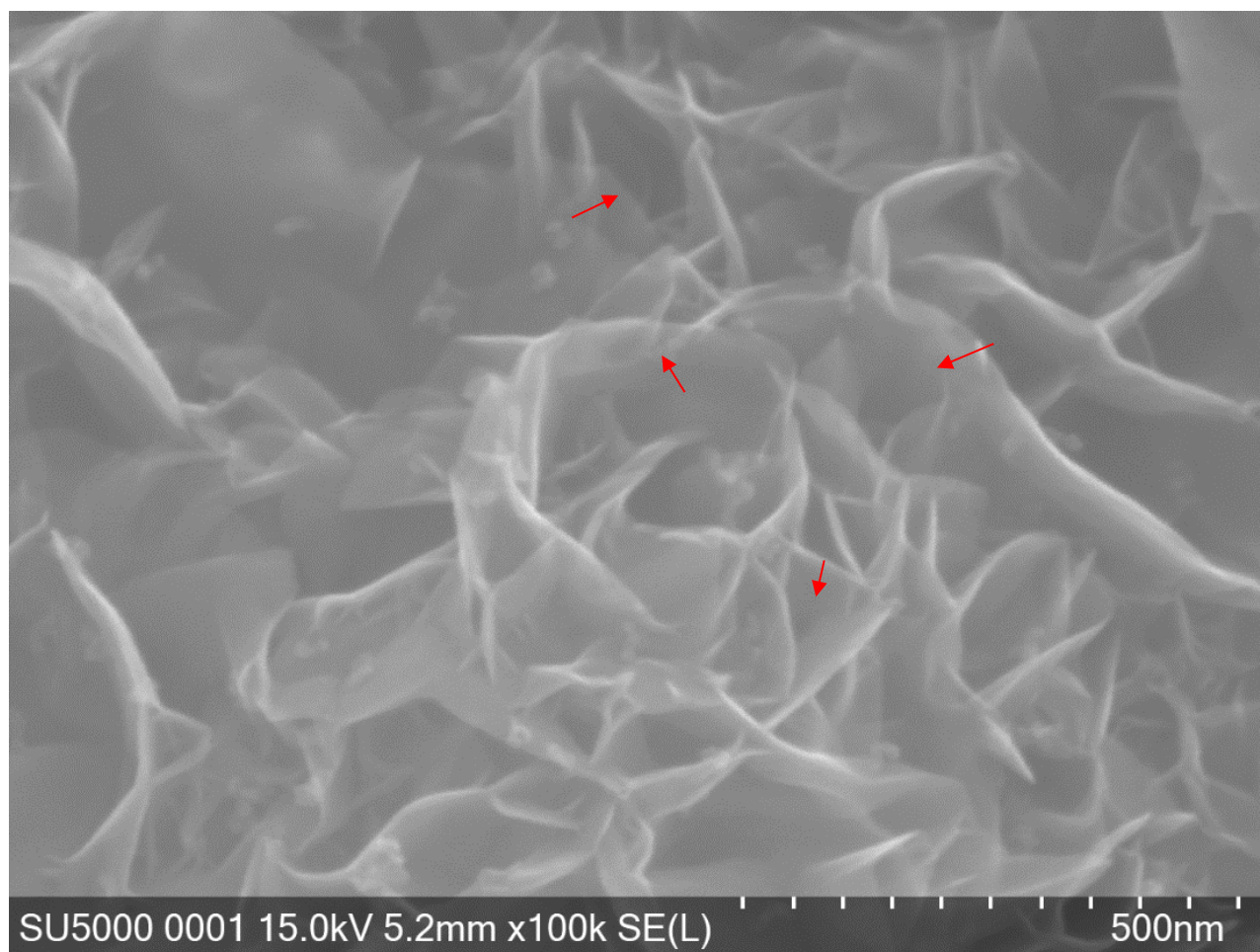


**Figure S6.** SEM micrograph of GNFs where a few transparent graphene layers are indicated by arrows.

## S6. Mechanical characterization of hybrid fibres via single carbon fibre tensile strength measurements

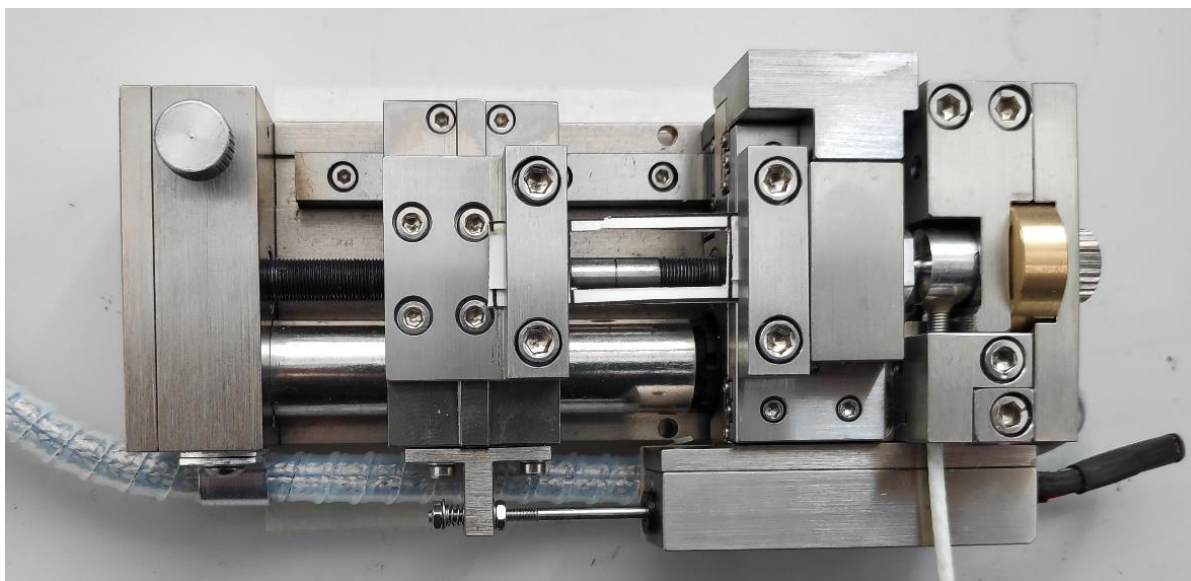


**Figure S7.** The experimental set-up (Deben UK) used for the single carbon fibre tensile strength measurements.

### *S6.1 Preparation and testing of specimens*

A single fibre, carefully separated from the GNFs/CF yarn, was fixed at the centre axis of a window paper holder (200 gr A4 paper) by mounting its ends, using a cyanoacrylate adhesive (Loctite 401). The carbon fibre was aligned with the axis of the cross-head of the tester with great care, in order to accomplish a uniform stress state over the cross-section of the fibre. Once the sample was secured both sides of the paper holder were cut carefully at the mid-gage as shown in **Figure S8**, leaving the fibre freestanding between the clamps, and then tensile test began.

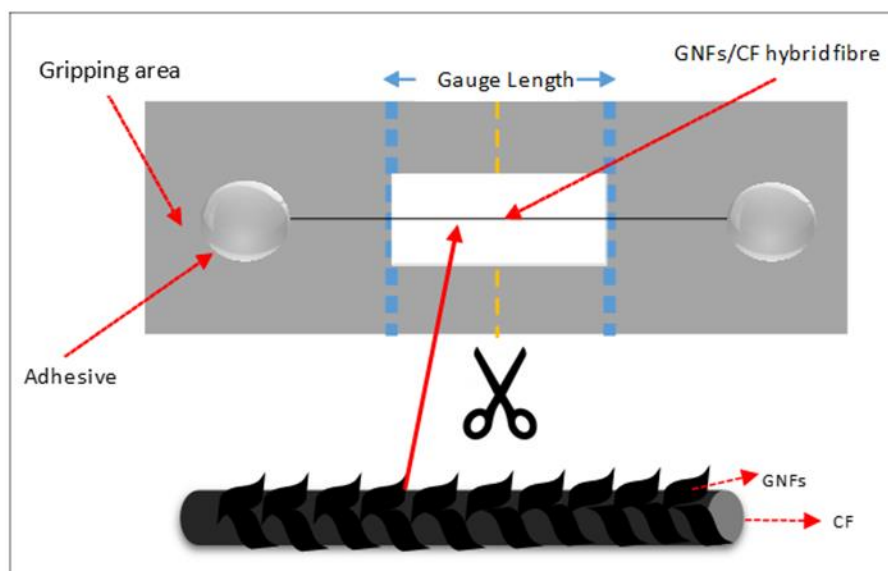


**Figure S8.** Schematic of the mounting paper for single fibre tensile strength measurement.

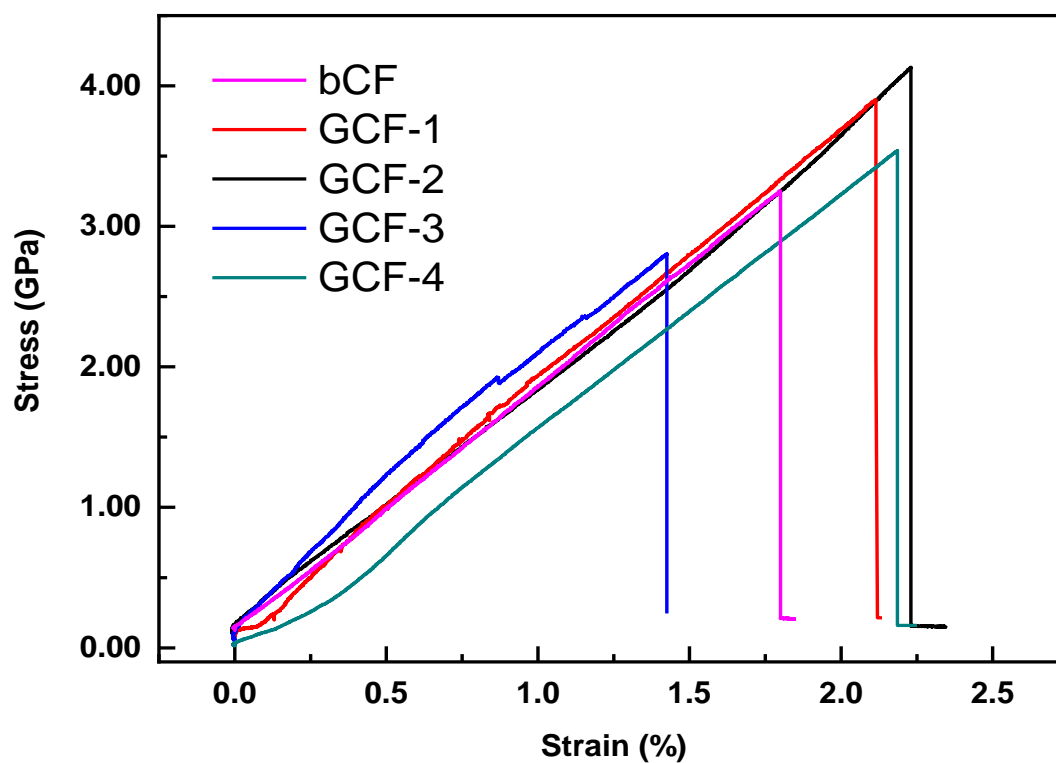


**Figure S9.** Representative stress-strain curves for all fabricated samples.

## S7. Mechanical characterization of hybrid fibres via Single Fibre Fragmentation measurement

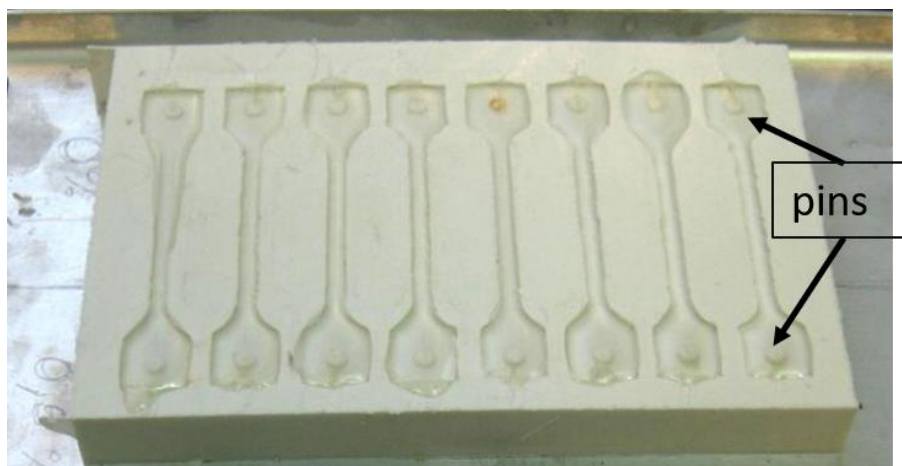


**Figure S10.** Silicon rubber mould used for the fabrication of single fibre model composites specimens.

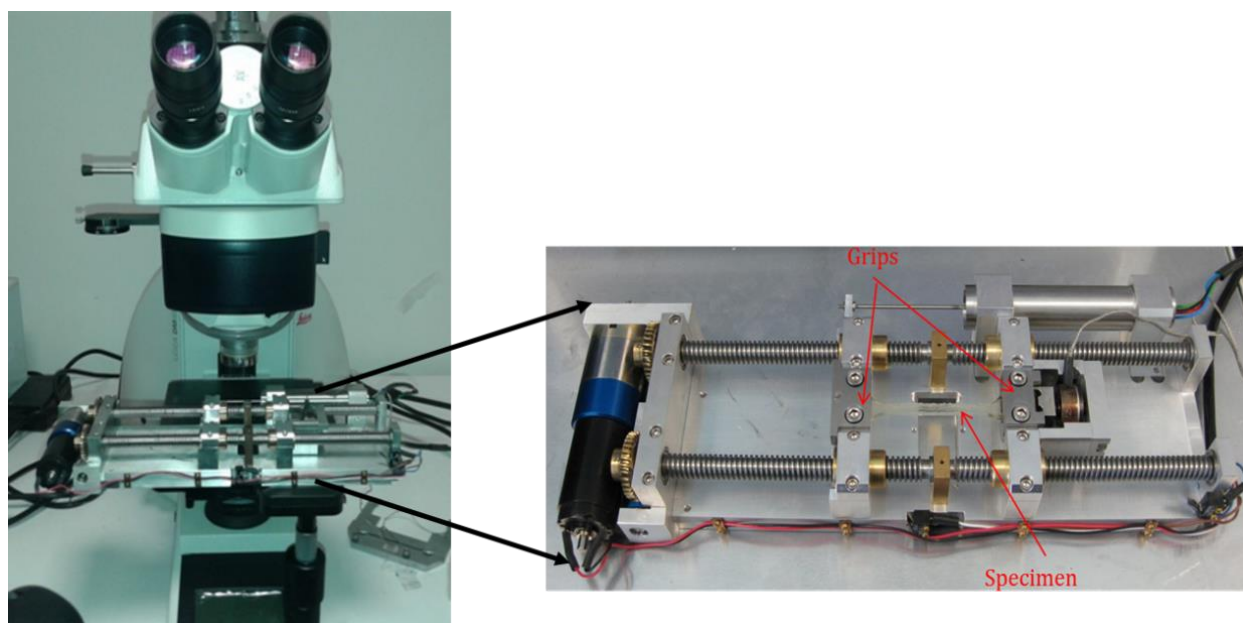


**Figure S11.** The experimental set-up used for the Single Fibre Fragmentation Tests (SFFT). The custom-made, horizontal tensile stage (right) placed under the Leica DM-4000M polarized optical microscope (left).

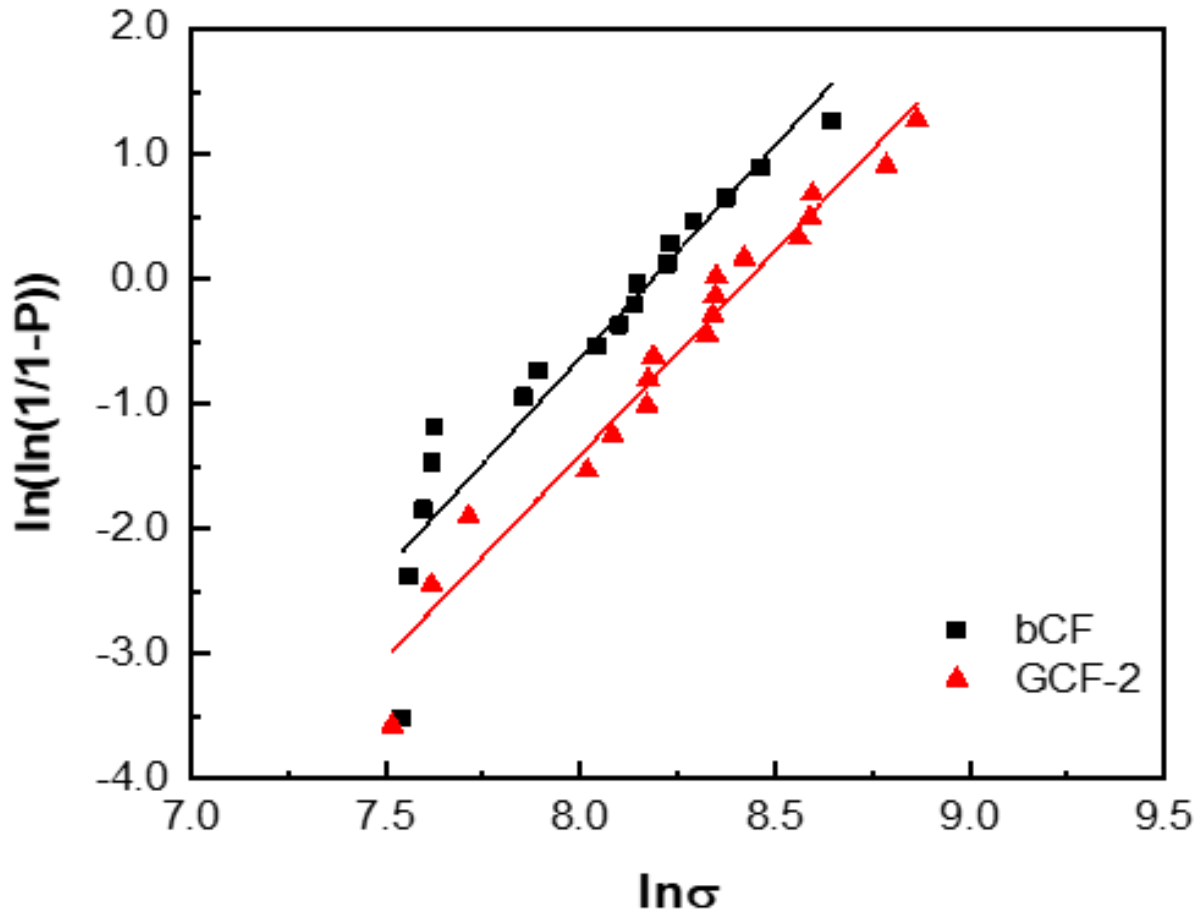


**Figure S12.** Weibull plots for the bCF and the GCF-2.

The calculated Weibull shape and scale parameters for the bCF and the GCF-2 were 3.39, 3589.0 and 3.25, 4591.7 respectively. These values were subsequently used for the evaluation of the bCF and GCF-2 strengths at the small fragment lengths observed during the SFFT. The results indicated a 101.5% increase in the IFSS of the GCF-2 in comparison to the bCF as summarized in **Table S3**.

**Table S3.** Fabrication conditions of hybrid fibres, their thickness, GNF length, Tensile Strength ( $\sigma_f$ ), Young's Modulus (E) and Interfacial shear strength (IFSS) at single fibre level. Error bars represent standard deviation from at least 20 independent measurements.

	bCF	GCF-1	GCF-2	GCF-3	GCF-4
<b>Growth time (min)</b>	0	3 min	3 min	3 min	3 min
<b>Power (W)</b>	0	500	800	950	800
<b>Temperature (°C)</b>	0	600	600	600	300
<b>Coating thickness (<math>\mu\text{m}</math>)</b>	0	0.28	1.10	0.35	0.065
<b>GNFs length (nm)</b>	0	$110 \pm 25$	$287 \pm 75$	$197 \pm 40$	$200 \pm 59$
<b><math>\sigma_f</math> (GPa)</b>	$3.2 \pm 0.3$	$3.9 \pm 0.2$	$4.1 \pm 0.3$	$2.8 \pm 0.2$	$3.6 \pm 0.3$
<b>E (GPa)</b>	$178 \pm 4$	$155 \pm 9$	$164 \pm 9$	$180 \pm 8$	$169 \pm 8$
<b>IFSS (MPa)</b>	$15.1 \pm 4.3$	-	$30.4 \pm 3.6$	-	-

## S8. Electrical conductivity measurements

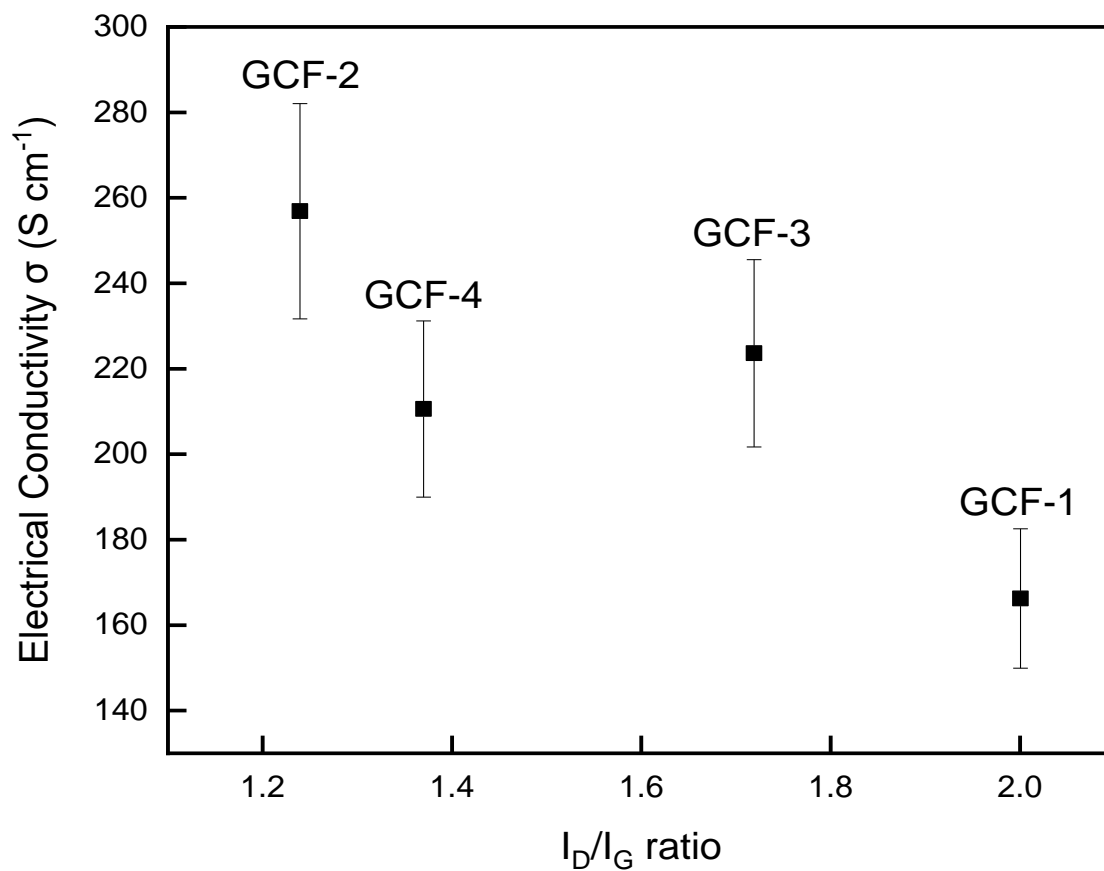


**Figure S13.** Electrical conductivity ( $\sigma$ ) of hybrid carbon fibres yarns as a function of D/G band ( $I_D/I_G$ ) intensity ratio. Error bars represent standard deviation from at least 20 independent measurements.

## S9. Electrochemical Characterization

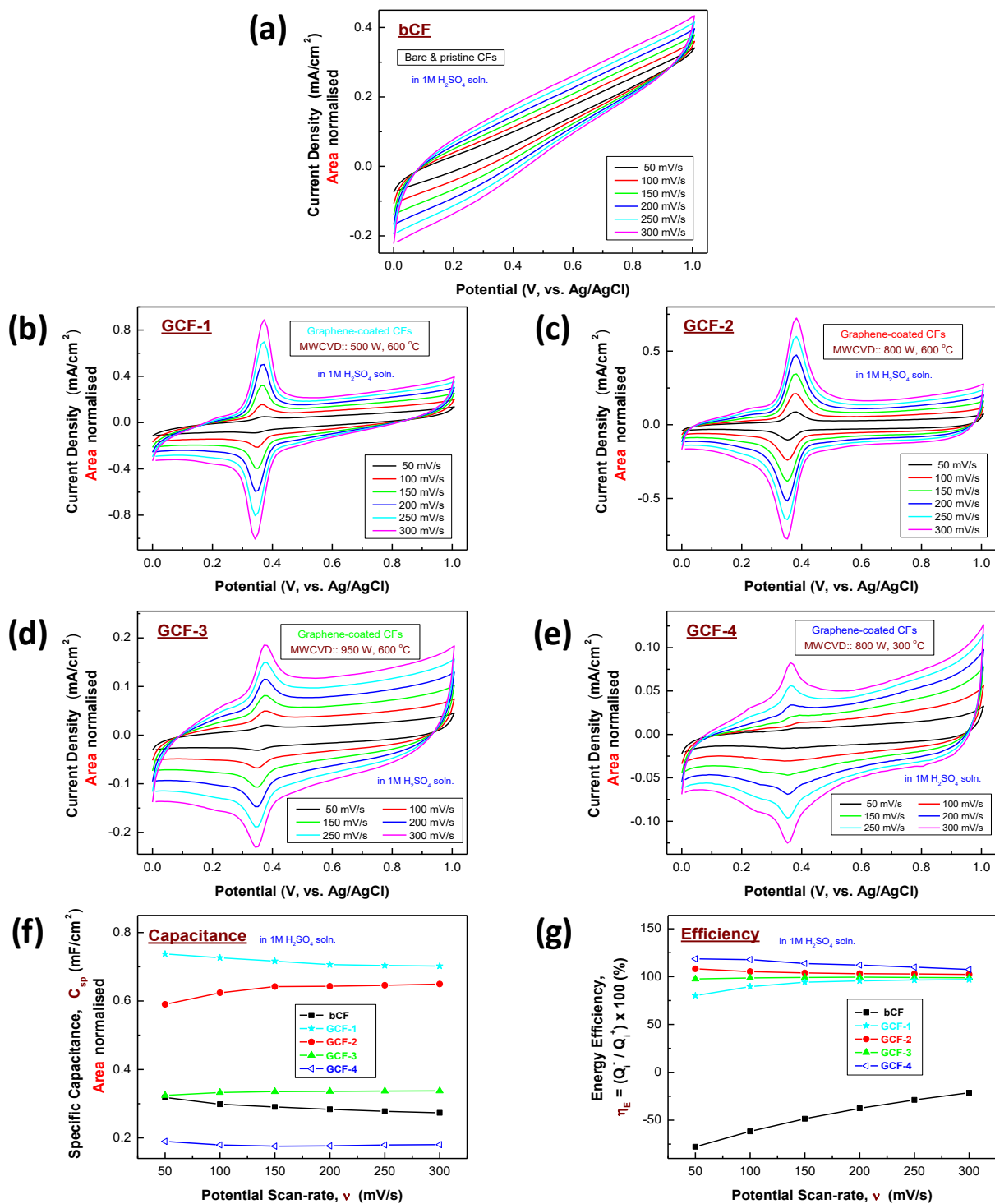


**Figure S14.** Plots of cyclic voltammograms as a function of potential scan rate, recorded in 1.0 M H<sub>2</sub>SO<sub>4</sub> electrolyte at the (a) bare (bCFs) and (b-e) graphene nanoflake coated carbon fibre yarn

(GCF) electrodes. (f) Areal specific capacitance ( $C_{sp}$ ) and (g) corresponding energy efficiency ( $\eta_E$ ) values, as a function of potential scan rate, derived from the CV curves, measured in 1.0 M  $\text{H}_2\text{SO}_4$  electrolyte.

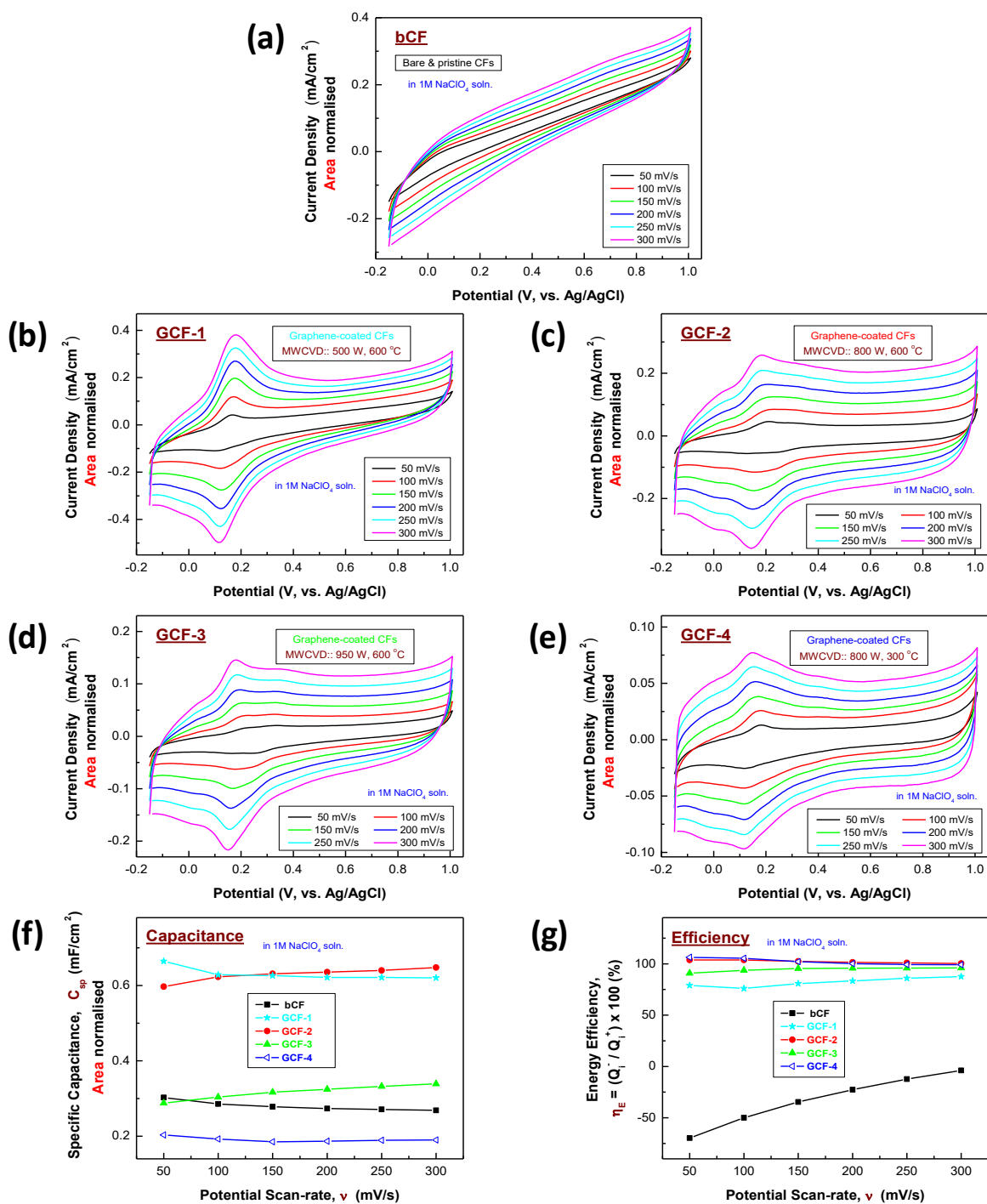


**Figure S15.** Plots of cyclic voltammograms as a function of potential scan rate, recorded in 1.0 M NaClO<sub>4</sub> electrolyte at the (a) bare (bCFs) and (b-e) graphene nanoflake coated carbon fibre yarn (GCF) electrodes. (f) Areal specific capacitance ( $C_{sp}$ ) and (g) corresponding energy efficiency

( $\eta_E$ ) values, as a function of potential scan rate, derived from the CV curves, measured in 1.0 M NaClO<sub>4</sub> electrolyte.

### S9.1 Development of redox peaks during initial conditioning

**Figure S16** presents the development of the redox peaks during 10 conditioning cycles. The redox peaks, in the region of  $\sim 0.36\text{V}$  vs Ag/AgCl, during the first scan are small but are increased during subsequent scans and are attributed to the formation of quinonodal ( $\text{C}=\text{O}$ ) groups on graphitic edges surfaces of GNFs.

The redox reactions are described by the following equation:

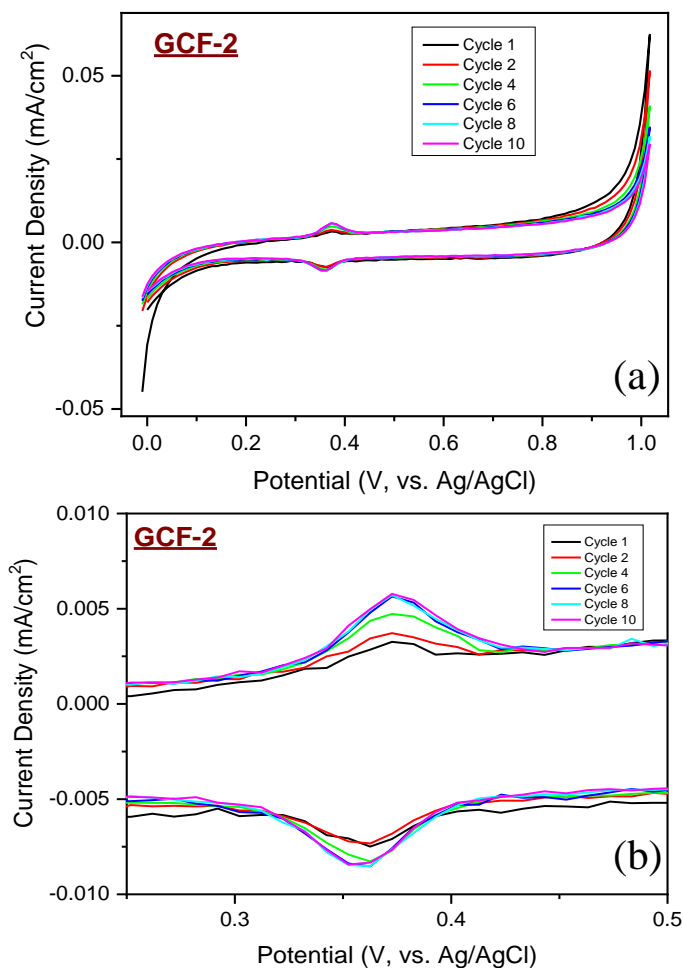


**Figure S16.** (a) Plots of cyclic voltammograms for the first 10 cycles, recorded in 1.0 M  $\text{H}_2\text{SO}_4$  electrolyte, at a scan rate of 10mV/s, on GCF-2 graphene nanoflake coated carbon fibre yarn electrode. (b) magnified version of redox peaks present in (a).

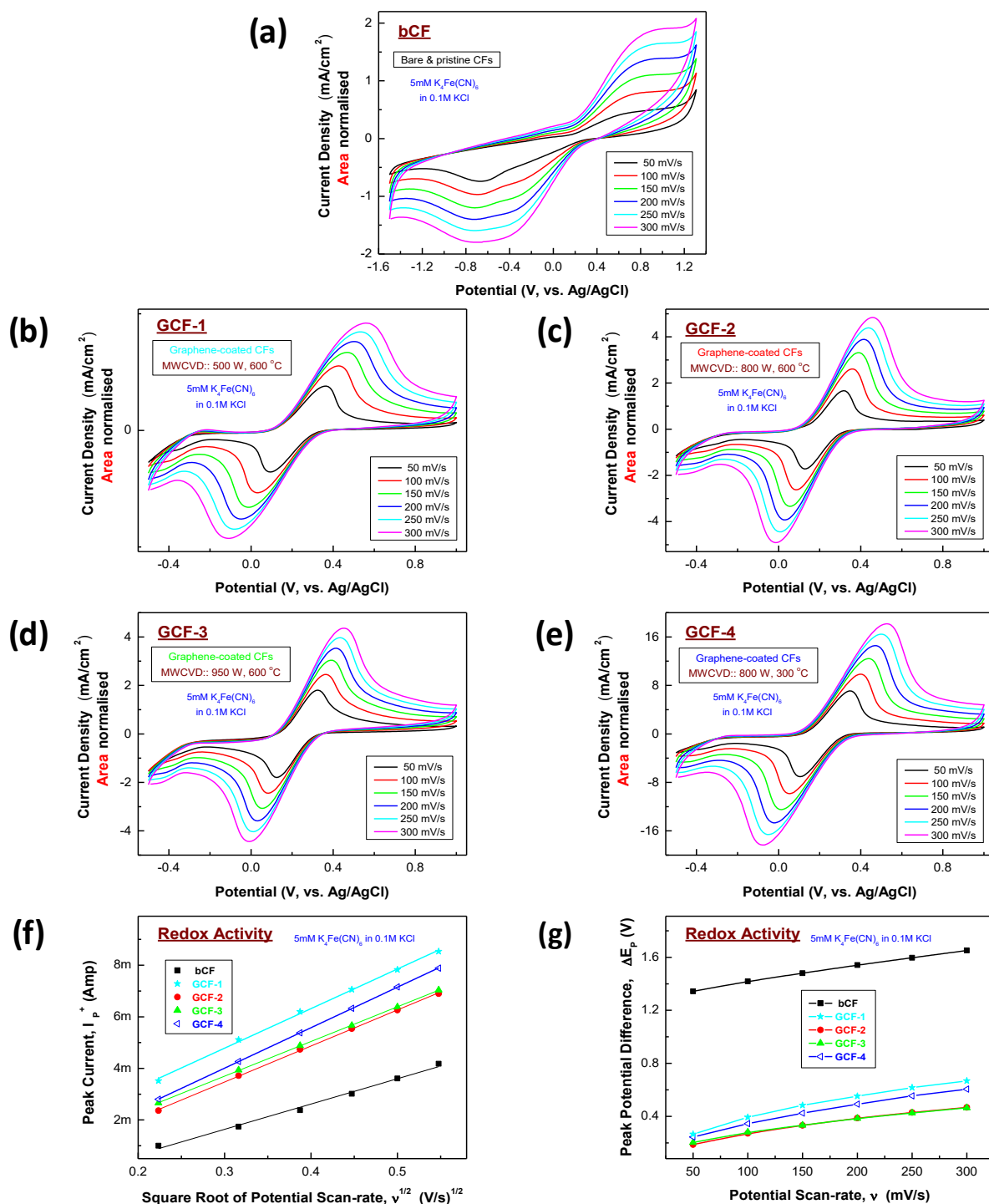


**Figure S17.** Plots of cyclic voltammograms as a function of potential scan rate, recorded in 5mM  $K_4Fe(CN)_6$  in 0.1M KCl solution at the (a) bare (bCFs) and (b-e) graphene nanoflake coated (GCFs) carbon fibre yarn (GCF) electrodes. (f) Plots with linear fitting of the  $Fe(CN)_6^{3-/4-}$  redox

peak currents ( $I_p$ ) with the square root of potential scan rates ( $\nu^{1/2}$ ) for bCFs and GCFs electrodes.

(g) The respective redox peak potential difference,  $\Delta E_p$ , values as a function of potential scan rate, for the redox activity of  $\text{Fe}(\text{CN})_6^{3-/4-}$ .

**Table S4.** Electroactive surface area (ESA), Geometric surface area (GA) and Efficiency parameter  $\eta_{SA}$  of GNFs/CF hybrid yarn electrodes.

	ESA (cm <sup>2</sup> )	GA (cm <sup>2</sup> )	$\eta_{SA}$ %
<b>bCFs</b>	2.6	2.2	118
<b>GCF-1</b>	4.1	1.8	223
<b>GCF-2</b>	3.7	1.3	263
<b>GCF-3</b>	3.6	1.6	225
<b>GCF-4</b>	4.2	1.8	230

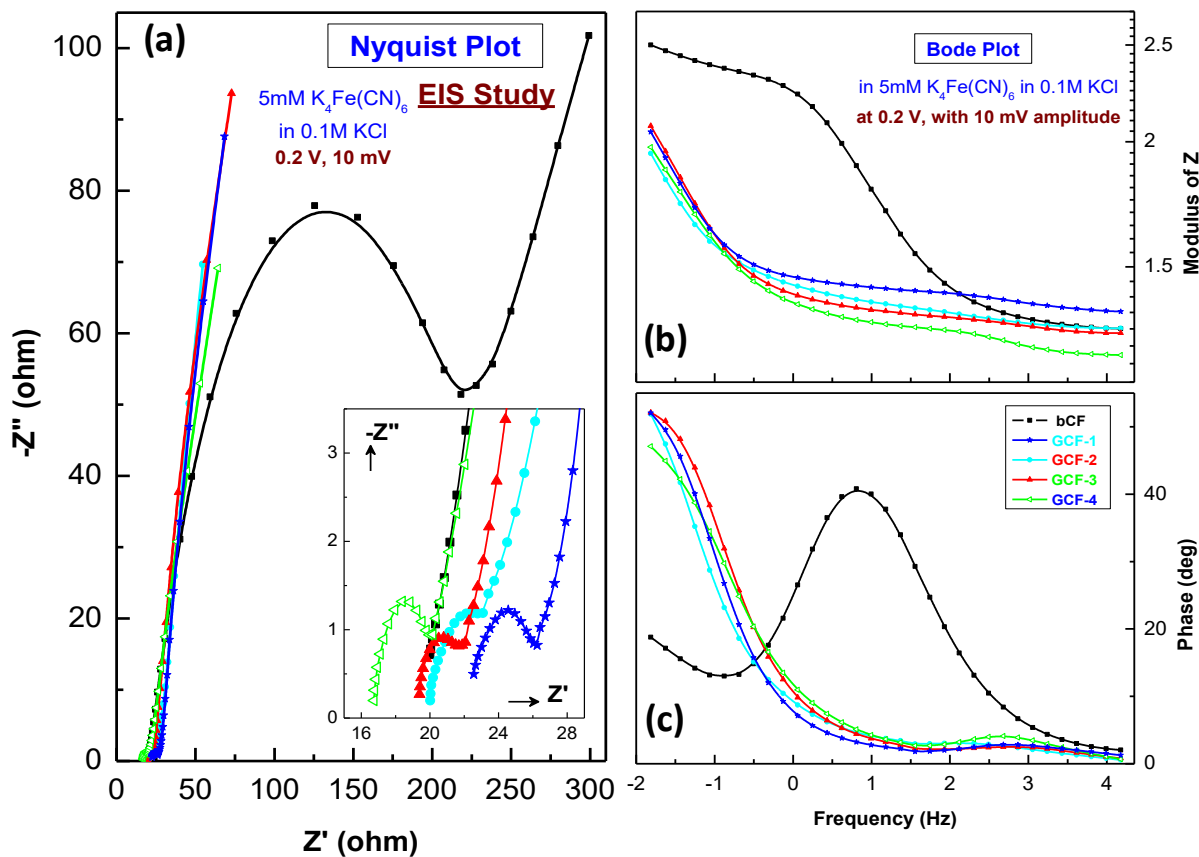


**Figure S18.** (a) Comparison of Nyquist plots for the bare (bCFs) and graphene nanoflake coated carbon fibre yarn (GCF) electrodes, recorded in 5mM  $K_4Fe(CN)_6$  in 0.1M KCl solution. The inset at the bottom shows a magnified view of the Nyquist plots close to the origin. Corresponding Bode plots of (b) modulus of  $Z$  and (c) phase as a function of frequency are presented.